# Climate Change in Mechanical Systems: The Snapshot View of Parallel Dynamical Evolutions

**Daniel Janosi** ( daniel.janosi@ttk.elte.hu )
Eotvos Lorand Tudomanyegyetem Termeszettudomanyi Kar https://orcid.org/0000-0002-6138-3610
**Gyorgy Karolyi**
Budapest University of Technology and Economics: Budapesti Muszaki es Gazdasagtudomanyi Egyetem
**Tamas Tel**
Eotvos Lorand Tudomanyegyetem Termeszettudomanyi Kar

**Research Article**

**Keywords:** parameter drift, chaos theory, climate change, ensemble evolution, Lyapunov exponent, snapshot attractor, doubly transient chaos, parallel climate realizations, Smale horseshoe, phase space structures

**Posted Date:** April 21st, 2021

**DOI:** https://doi.org/10.21203/rs.3.rs-427225/v1



**Version of Record:** A version of this preprint was published at Nonlinear Dynamics on November 1st, 2021. See the published version at https://doi.org/10.1007/s11071-021-06929-8.

# Abstract

We argue that typical mechanical systems subjected to a monotonous parameter drift whose time scale is comparable to that of the internal dynamics can be considered to undergo their own climate change. Because of their chaotic dynamics, there are many permitted states at any instant, and their time dependence can be followed - in analogy with the real climate - by monitoring parallel dynamical evolutions originating from different initial conditions. To this end an ensemble view is needed, enabling one to compute ensemble averages characterizing the instantaneous state of the system. We illustrate this on the examples of (i) driven dissipative and (ii) Hamiltonian systems and of (iii) non-driven dissipative ones. We show that in order to find the most transparent view, attention should be paid to the choice of the initial ensemble. While the choice of this ensemble is arbitrary in the case of driven dissipative systems (i), in the Hamiltonian case (ii) either KAM tori or chaotic seas should be taken, and in the third class (iii) the best choice is the KAM tori of the dissipation-free limit. In all cases, the time evolution of the chosen ensemble on snapshots illustrates nicely the geometrical changes occurring in the phase space, including the strengthening, weakening or disappearance of chaos. Furthermore, we show that a Smale horseshoe (a chaotic saddle) that is changing in time is present in all cases. Its disappearance is a geometrical sign of the vanishing of chaos. The so-called ensemble-averaged pairwise distance is found to provide an easily accessible quantitative measure for the strength of chaos in the ensemble. Its slope can be considered as an instantaneous Lyapunov exponent whose zero value signals the vanishing of chaos. Paradigmatic low-dimensional bistable systems are used as illustrative examples whose driving in (i, ii) is chosen to decay in time in order to maintain an analogy with case (iii) where the total energy decreases all the time.


# Full Text

This preprint is available for download as a PDF.

# Figures

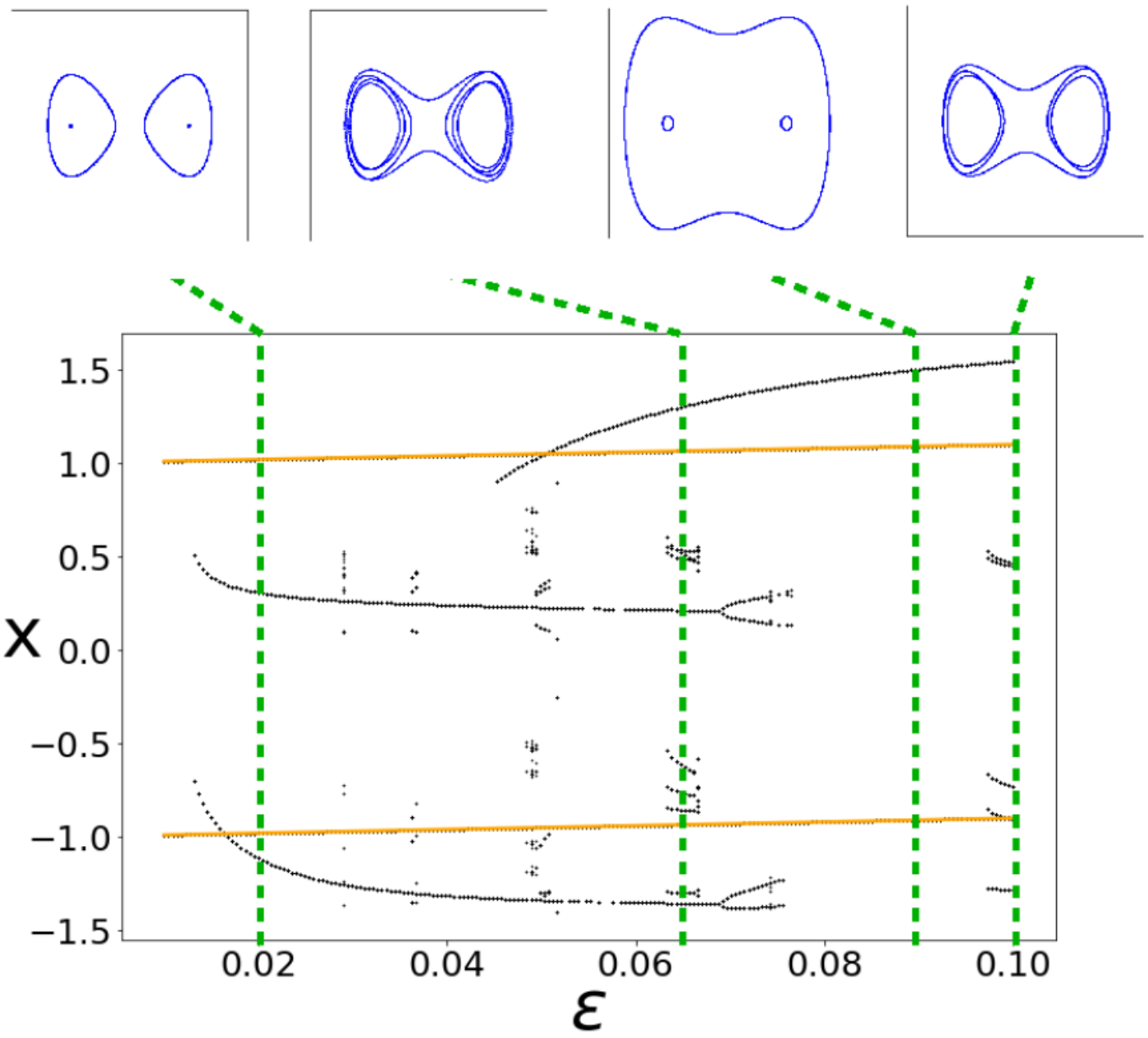


**Figure 1**

Bifurcation diagram of the driven Duffing system (1) with fixed driving amplitudes ε. The x coordinates on the attractors are plotted in the stroboscopic map (omitting the first 450 iterations). The upper and lower straight branches indicate the existence of two period-1 attractors whose locations tend to the potential minima for vanishing amplitude. They overlap with the orange lines, which correspond to equation (7) for α =0. There exist two more period-1 attractors (bent curves) representing large oscillation in each potential well which are born in a saddle-node bifurcation at ε ≈ 0:01. A third one appears at about ε = 0:05 and describes a period-1 oscillation surrounding both wells. The phase space view of these orbits and of a period 5 and 7 attractor existing in relatively long e intervals are indicated in insets.

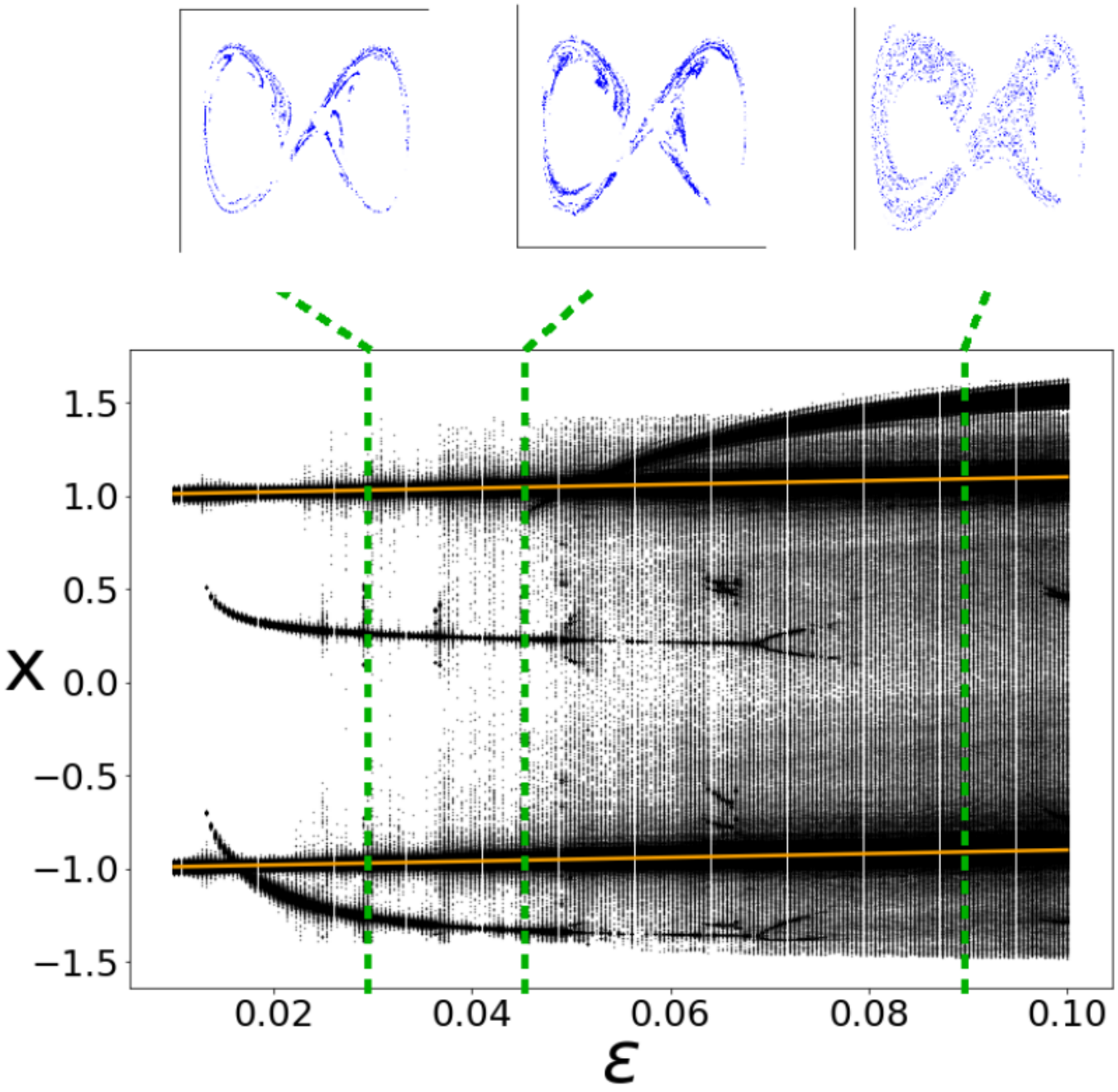


**Figure 2**

Bifurcation diagram including long-lived transients. Similar to Fig. 1, but only the first 50 iterates of the trajectories are omitted. 900 initial conditions have been followed distributed uniformly in $-1 < x < 1$ for any fixed driving amplitude. Note how much more empty the traditional diagram in Fig. 1 is. The stroboscopic view of a few chaotic saddles belonging to the e values 0.03, 0.045 and 0.09 are shown in insets.

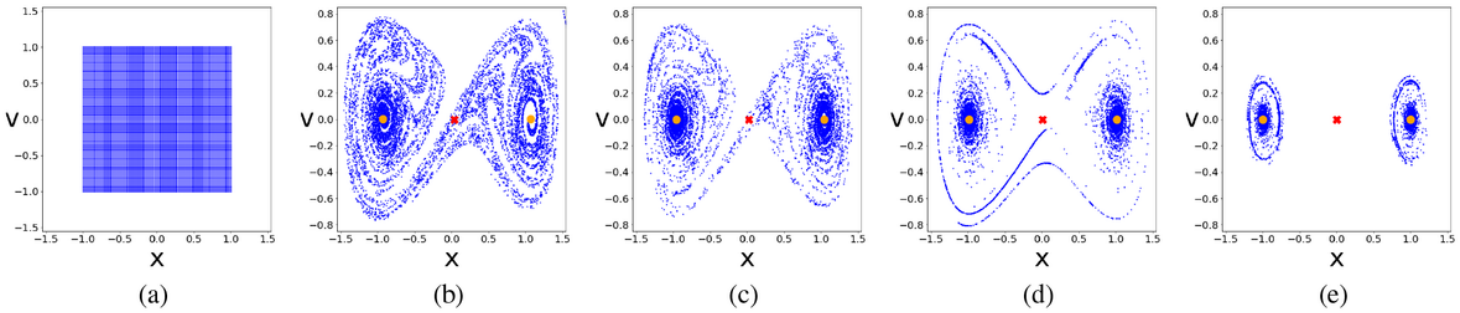


## Figure 3

Snapshot attractors of the dissipative Duffing system. An extended ensemble of 10000 points initially forming a square in the range [-1;1] in both x and v (a) is subjected to the scenario ε0 = 0:1, β = 0:01, α ≈ 0:0003 (n0 = 50). Here and in all of the numerical examples shown, the frequency is ω = 1. (b)-(e): The evolution of the snapshot attractor, i.e., of the ensemble (blue dots), shown in the instances n = 15;30;45; 60, respectively. For completeness, the snapshot points determined in Section 2.2 are overlaid with the snapshot attractors at the corresponding instances. The SHP of (5) and the SNPs of (6) appear in red and orange, respectively. The last image of n = 60 shows the snapshot attractor after n' = 10 steps on the plateau of zero driving.

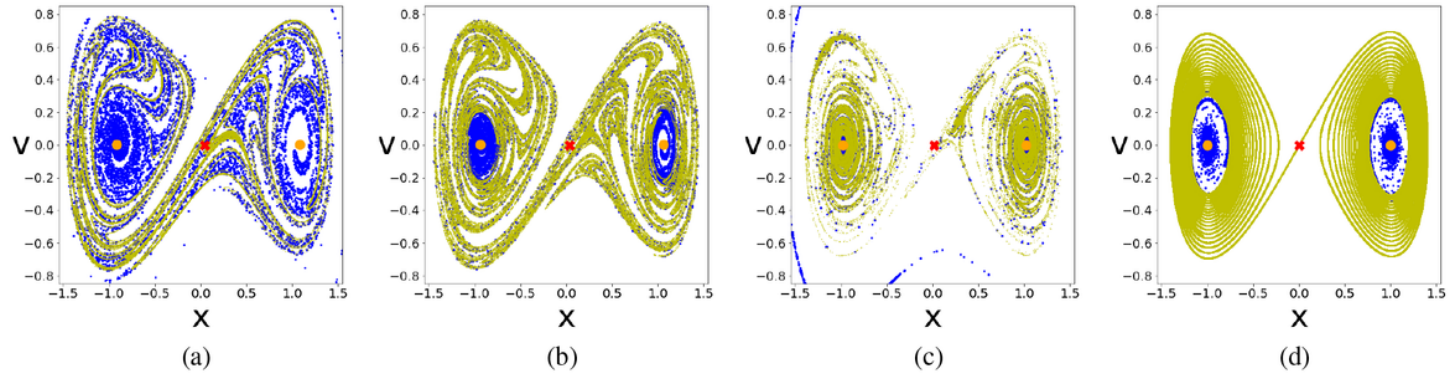


## Figure 4

Snapshot attractor (blue) and snapshot unstable manifold (yellow) in the scenario ε0 = 0:1, β = 0:01, α ≈ 0:0003 (n0 = 50), the same as in Figure 3. Here we display the steps n = 10;20;40; 60, respectively in (a)-(d). In (a)-(c), the yellow unstable manifold was originated at n = 5 in the form of a section of length dl = 0:2 along the diagonal crossing x*H:5, consisting of 100000 points, while in (d) it was generated as usual: by iterating a short line segment crossing the origin. The SHP of (5) (red) and the SNPs of (7) (orange) are displayed as well.

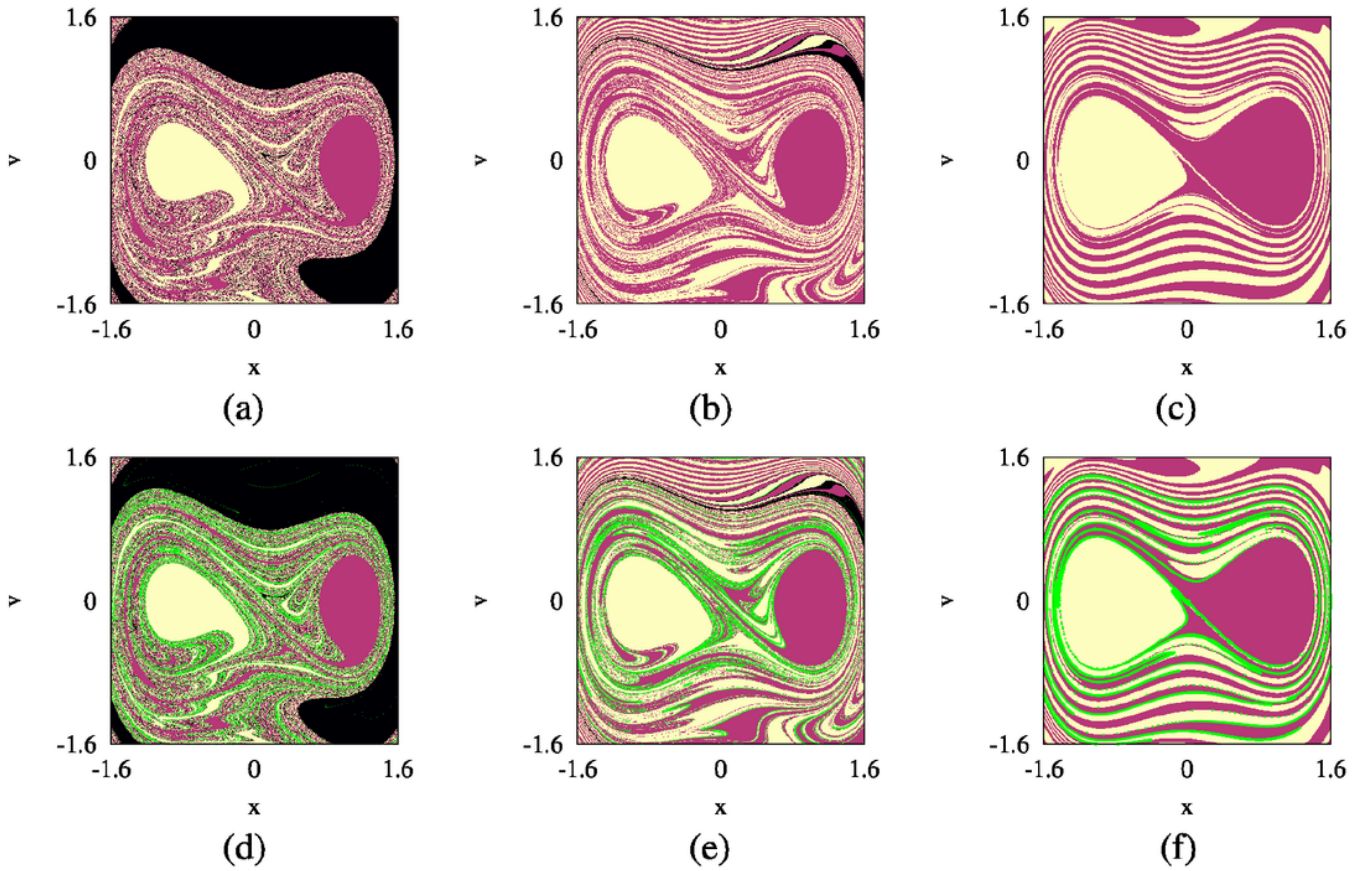


## Figure 5

Basins of attraction for the two stable fixed points (±1;0) starting the trajectories at steps (a) n = 10, (b) n = 25 and (c) n = 40 using the scenario ω = 1, ε0 = 0:1, β = 0:01, a ≈ 0:0003 (n0 = 50). Black areas indicate initial conditions not reaching the 10−2 vicinity of any of the attractors in 300 time units. In the bottom row we see the basins overlaid with the green instantaneous stable manifolds belonging to the same instants, initiated from the unstable fixed point (0;0) at n0 = 50.

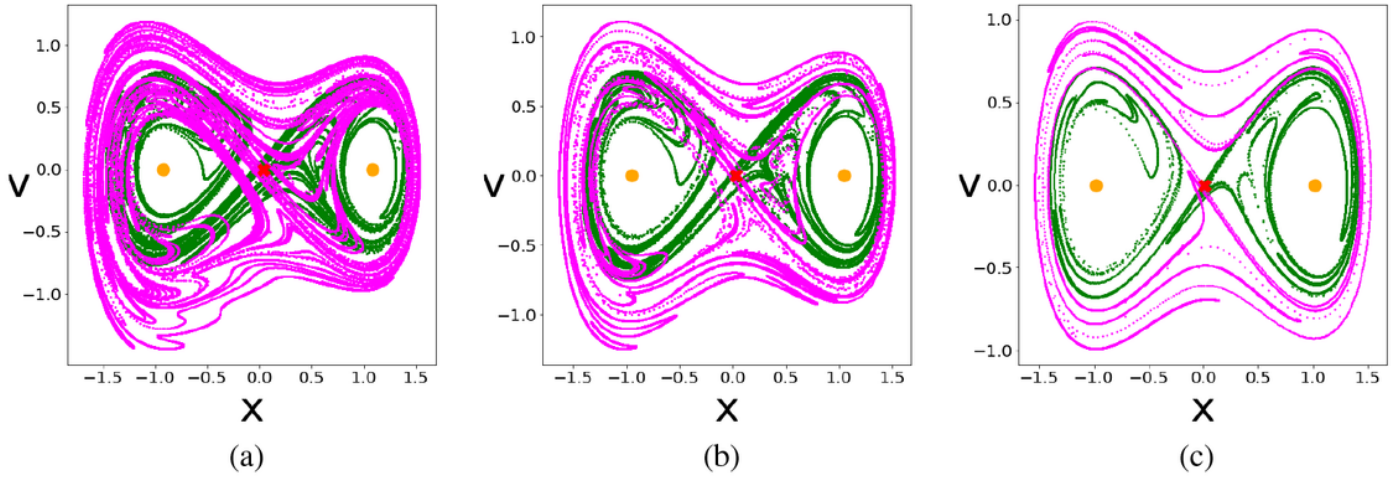


## Figure 6

Snapshot horseshoe structure at steps 10, 25 and 40, of the same scenario used so far, amounting to instantaneous amplitudes ε(t) = 0:08, 0.05 and 0.02, respectively. Here ñ = 5 is taken, that is, the stable manifold (pink) is initiated about x*H,15 and was iterated back to n = 10 in (a), n = 30→25 applies in (b) and n = 45→40 in (c), while for the unstable evolutions (green) n = 5→10 was taken in (a), n = 20→25 in (b) and n = 35→40 in (c). Observe that at the beginning of the scenario the area where the two manifolds cross is of considerable extension, while near the end of the ramp it shrinks to a few points about the origin. The SHP and the SNPs of (5) and (7), respectively are also displayed (red and orange).

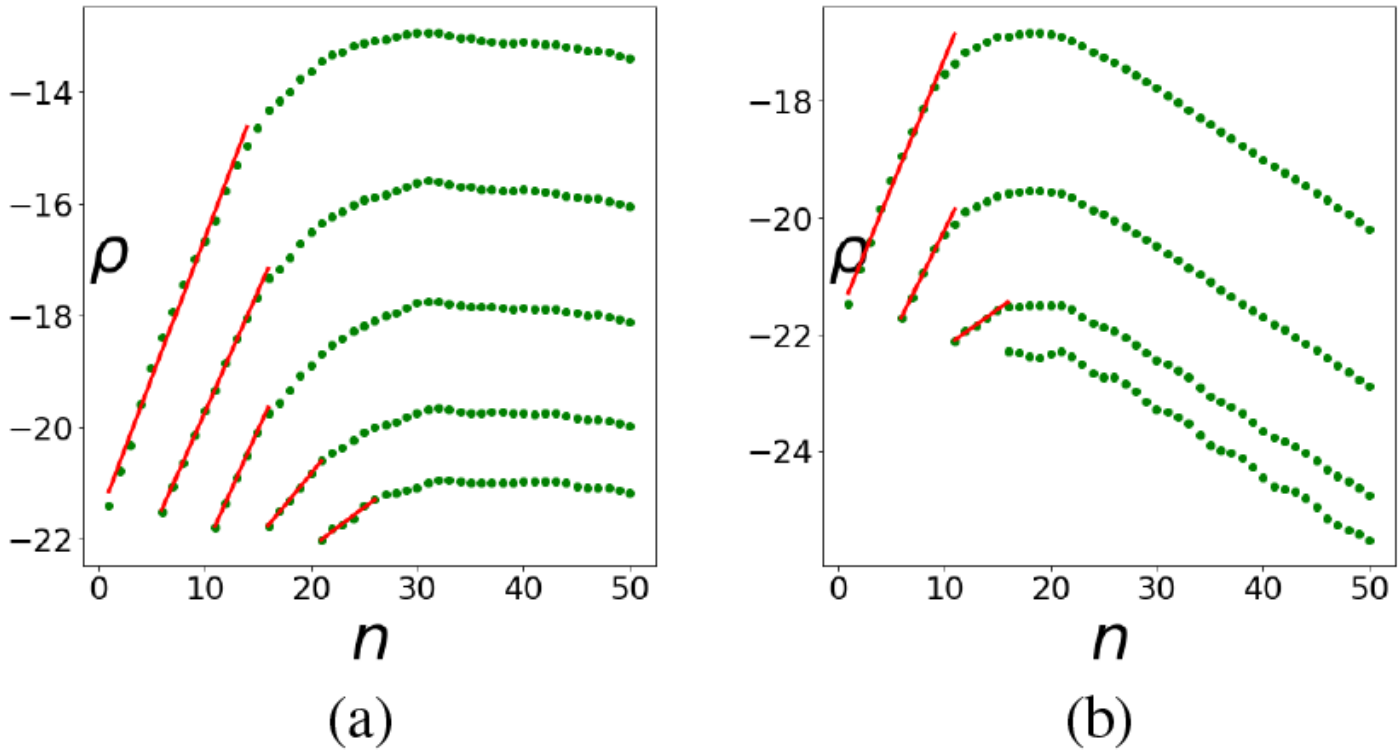


**Figure 7**

Ensemble-averaged pairwise distance in the scenario used throughout this section, followed until the end of the ramp. (a) The slopes of the fitted red segments are 0:50±0:01, 0:43±0:05, 0:42±0:006, 0:22±0:008, 0:14±0:1 and represent the initial Lyapunov exponent of the snapshot attractors. Note that all curves reach their maxima at about n = 30. (b) The same graphs for β = 0:02 (all other scenario parameters are the same). Here the location of the maxima, signalling the disappearance of chaos is about n = 20. The slopes of the fitted lines from top to bottom are 0:44±0:01, 0:37±0:01, 0:13±0:06.

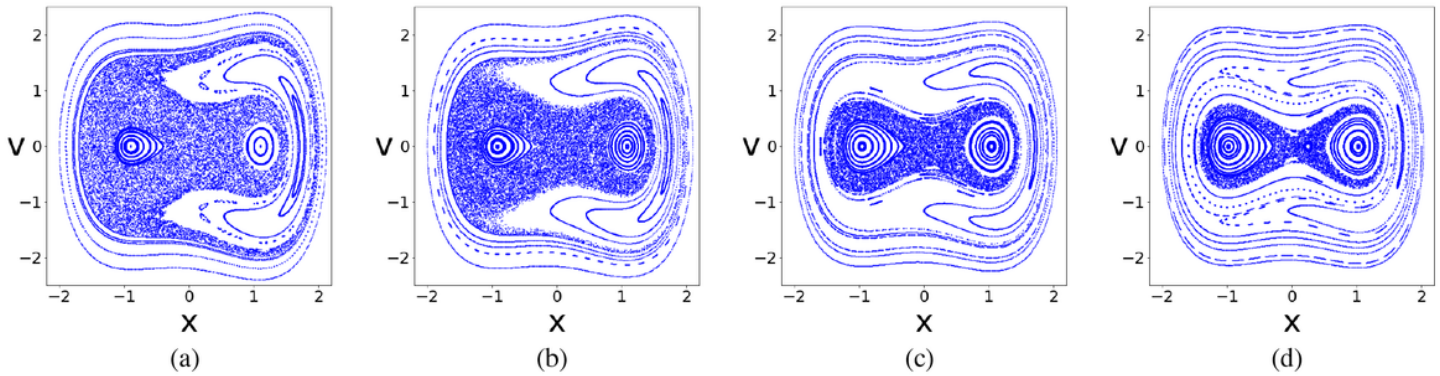


## Figure 8

Phase portraits of the stationary (α = 0) Hamiltonian Duffing-oscillator (9) displayed on a stroboscopic map for different fixed driving amplitudes ε(t) ≡ ε0 = 0:1;0:08;0:04 and 0:02 in panels (a), (b), (c), and (d), respectively. Trajectories are launched from 41 initial conditions distributed uniformly between −2 and +2 in x, with v = $\dot{x}$ = 0, and are followed in (9) for N = 1000 iterations.

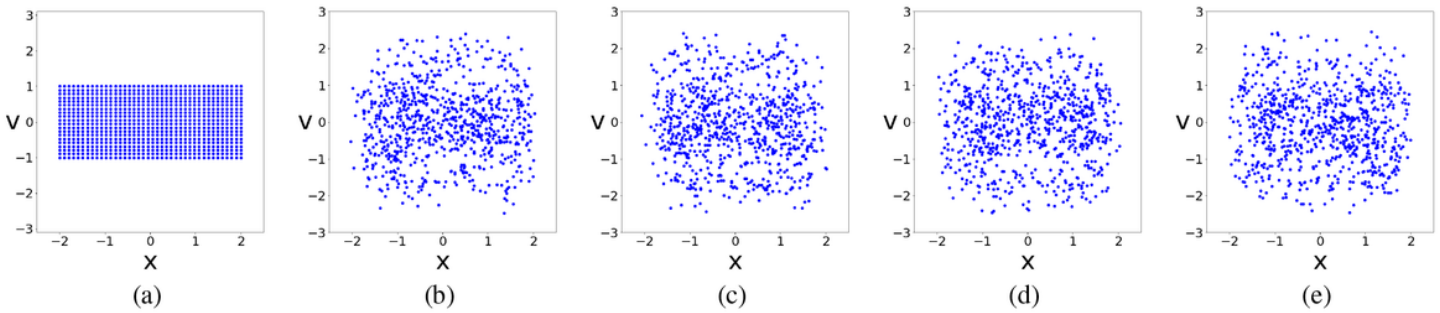


## Figure 9

Evolution of an extended ensemble of 800 points under (9) followed for 100 iterations of the stroboscopic map in the scenario ε0 = 0:1, n0 = 100 α ≈ 0:0002. The iteration numbers in panels (a)-(e) are n = 0;25;50;75; 100. The ensemble is initiated on the rectangle −2 to +2 in x, and −1 to +1 in v (panel a). Note that no structured pattern emerges in this extended ensemble. When following this scenario we are scanning through the stationary cases of all the panels of Fig.8.

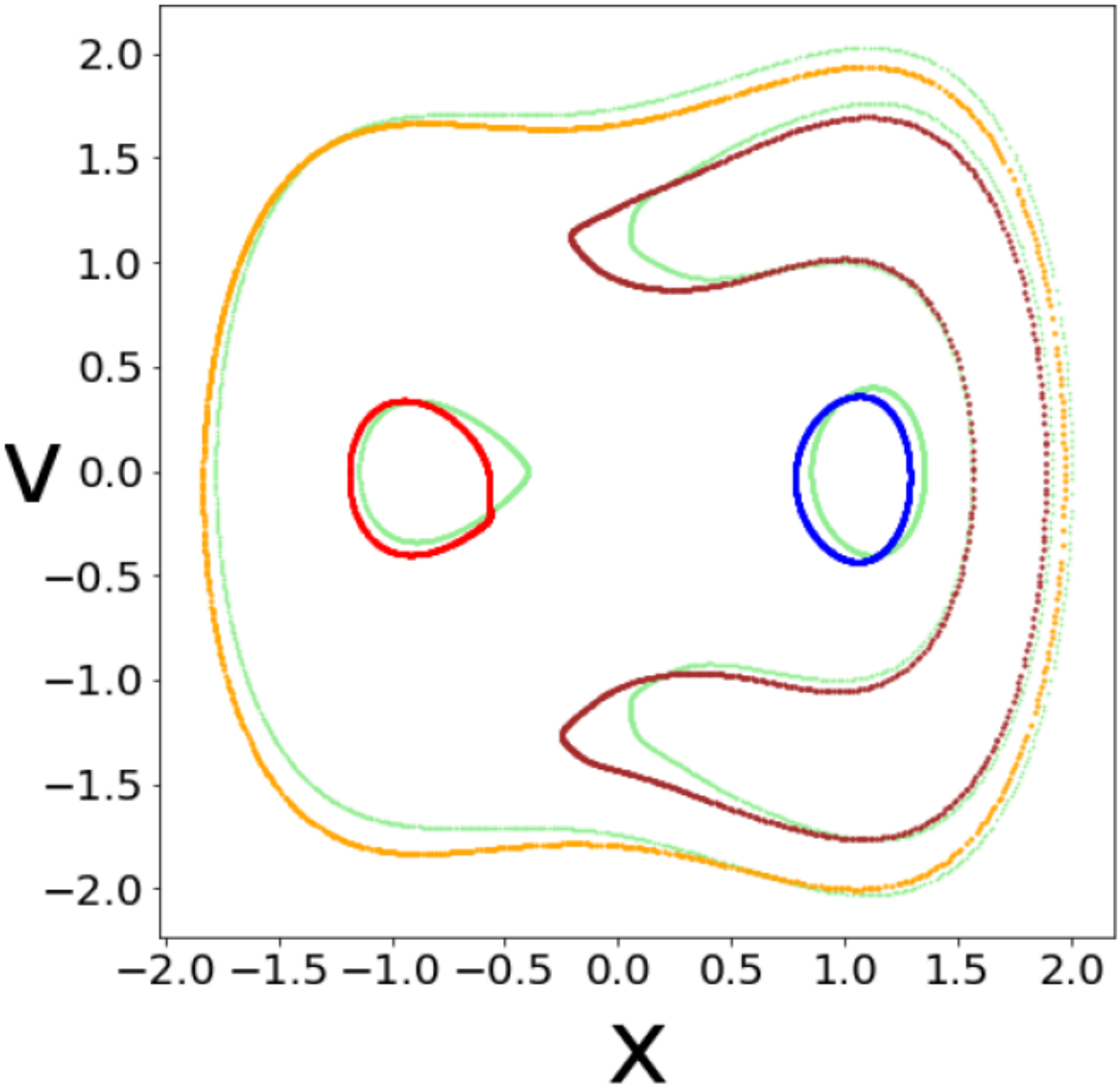


**Figure 10**

Four snapshot tori (colored curves) after 2 iterations. Four initial conditions x = −0:4;0:85;1:55;2 while v = 0 are iterated N = 1000 times under (9) with ε0 = 0:1, α = 0 forming the light green curves. Then the points consisting of these tori are taken as initial conditions, and iterated with scenario ε0 = 0:1, n0 = 5, α ≈ 0:003 over n = 2 periods, which leads to the snapshot tori shown here. It is remarkable to see that the tori remained closed (but deformed) curves.

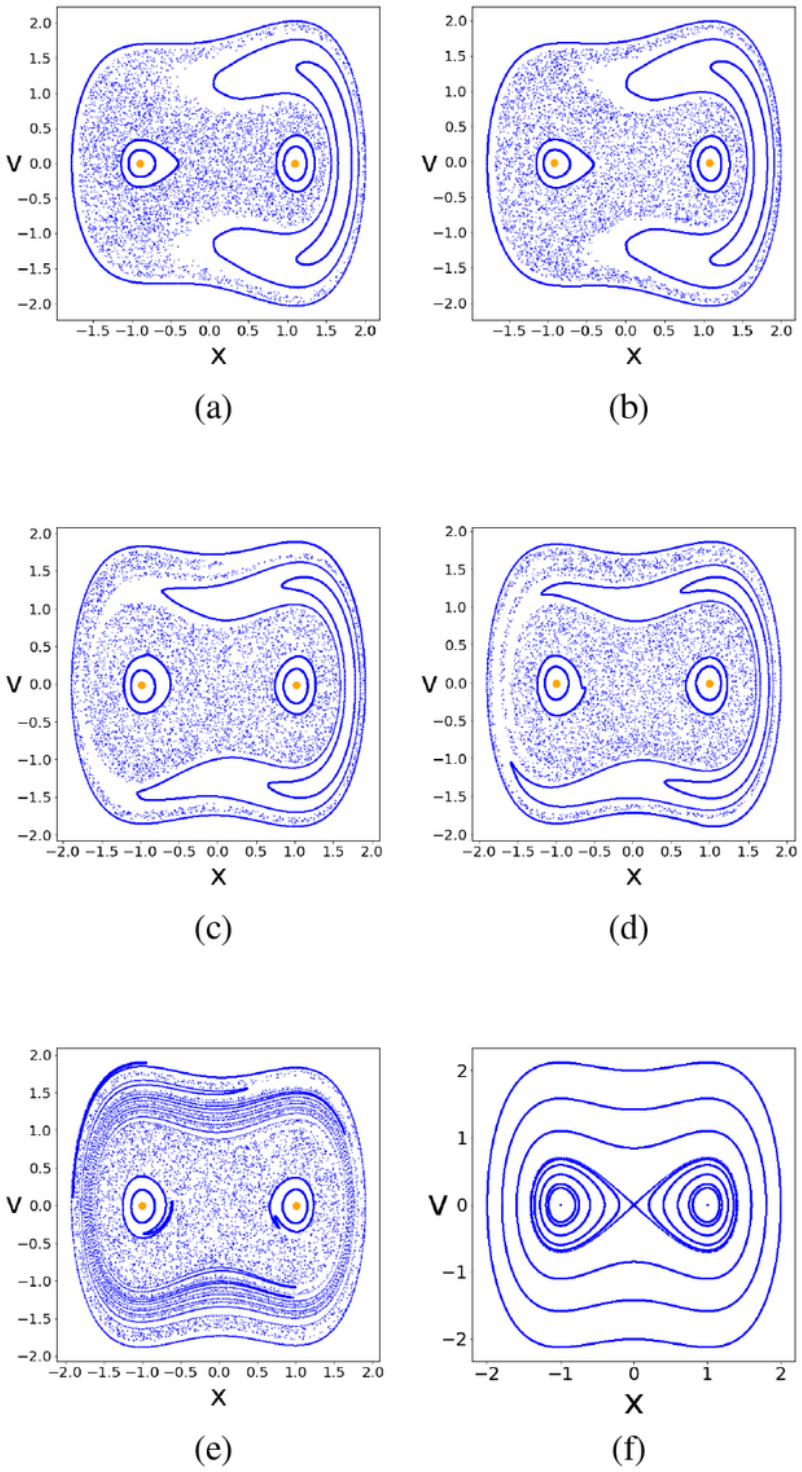


## Figure 11

Shape of the snapshot phase space along a scenario. (a) Frozen-in system with ε0 = 0:1, N = 5000 and the same initial conditions as in Fig.10, augmented with x0 = −0:7;0:95;1:65, three additional tori, and x0 = 0:1, representing the chaotic sea, while v0 = 0 for all. The elliptic fixed points are also displayed, in orange. (b)-(d) Results obtained with the scenario ε0 = 0:1, a ≈ 0:003, where the plateau of the undriven case is reached after n0 = 5 iterations. The snapshot phase space is shown at n = 1 (b), n = 4 (c) and n =

n0 = 5 (d). (e) The phase space at the iterate n = 15, meaning that 10 steps were spent in the undriven problem, n' = 10. (f) The phase portrait of the undriven (ε = 0) double well problem.

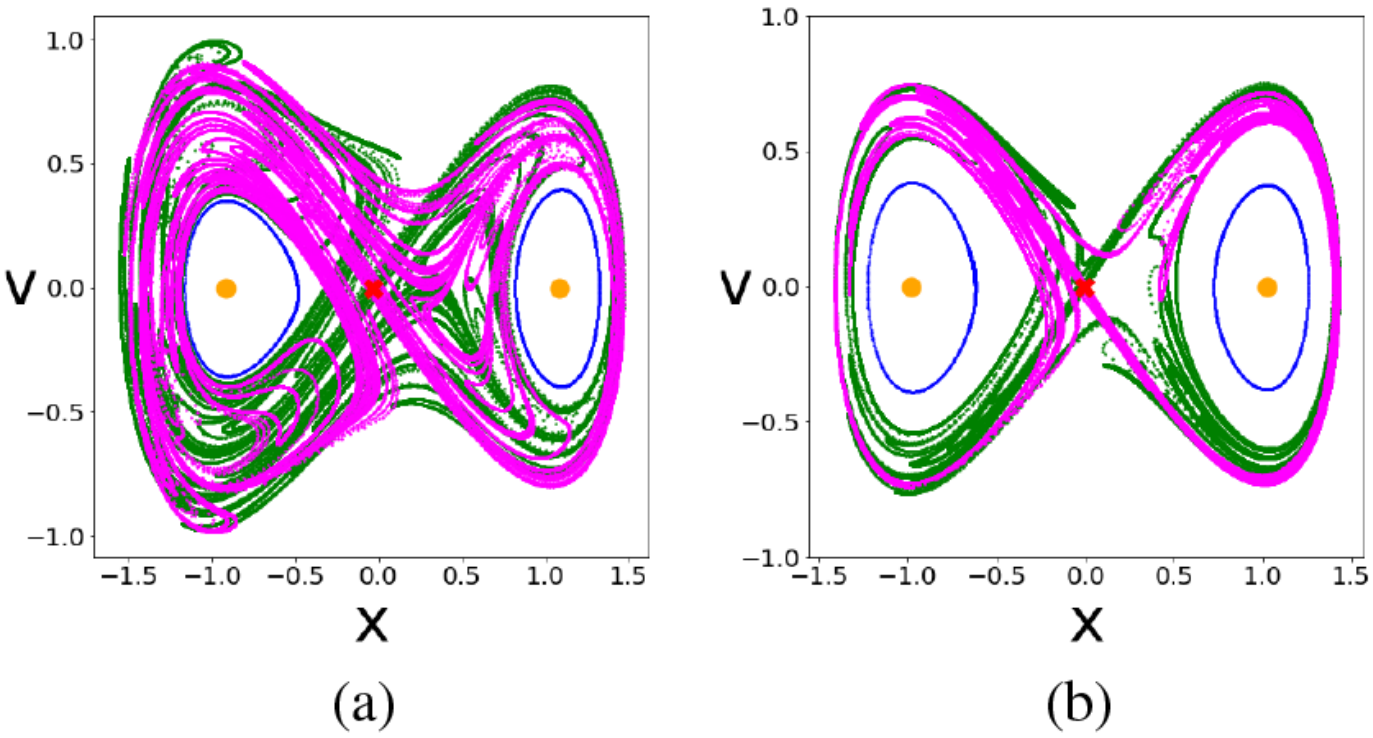


## Figure 12

Construction of two Hamiltonian snapshot horseshoe structures. (a) Stable manifold (pink) initiated at the hyperbolic point x*H,15 and unstable manifold (green) initiated at x*H,5. Both manifolds are iterated 5 times (ñ = 5) and then overlayed, thus showing the snapshot horseshoe of time instant n = 10, in the scenario ε0 = 0:1, n0 = 50, a ≈ 0:0003. (b) The snapshot horseshoe of n = 40 in the same scenario. The manifolds were iterated 5 times in this case too, thus the starting points are x*H,45 for the stable (pink) and x*H,35 for the unstable (green) manifold. Displayed in both cases are the snapshot tori of initial conditions x0 = −0:4;0:85, v0 = 0 (blue), the SEPs of (13) (orange) and the SHP of (11) (red). Observe that on (a) the structure is larger than that on (b), leading to the conclusion that during the scenario the region where true chaos is present, shrinks.

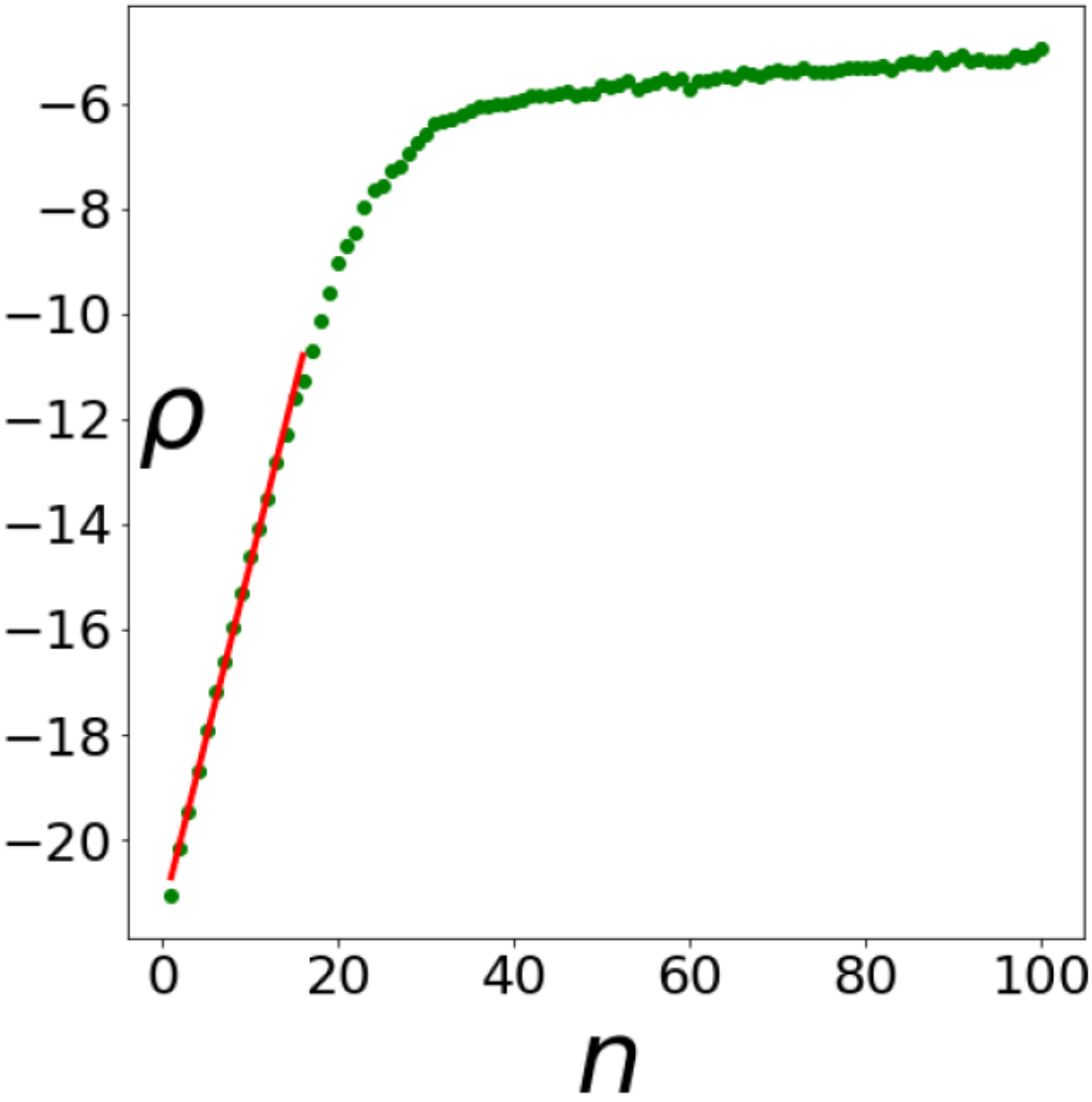


**Figure 13**

EAPD quantity corresponding to the chaotic sea of x0 = 0:1, v0 = 0, followed for 100 iterations with parameters ε0 =0:1, a ≈0:0003 (n0 =50). Since we are in a chaotic sea, the growth rate is exponential right away, becoming linear on the logarithmic scale used here. The slope of the fitted linear curve (red) gives us the Lyapunov value λ = 0:66±0:009. As one can see, the levelling off occurs at about ρ = −5, since the second half of the scenario is governed by the undriven problem. Also notable is that this flat part does not begin at n = n0 = 50 but much earlier, indicating that the scenario have already entered a region where the strength of chaos is diminishing.

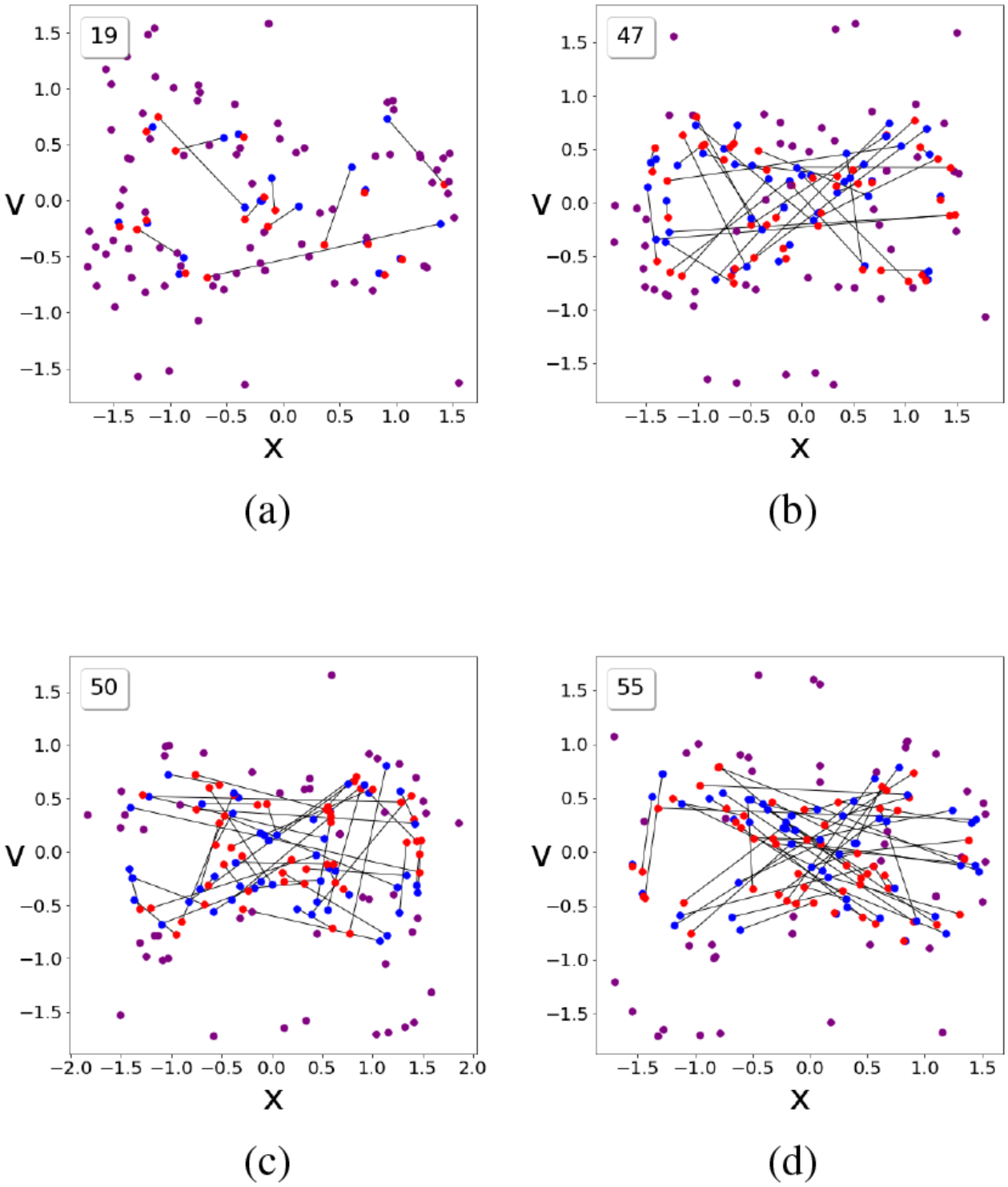


## Figure 14

The point pairs investigated in the scenario of Fig.13. The "close" pairs are colored purple while the others are colored blue and red and are connected by a black line. The number of "not close" pairs is given in the upper left corner. The images show the scenario at four different steps: (a) n = 20, (b) n = 30, (c) n = n0 = 50 and (d) n = 75. Observe that from n = 30, the number of connected points grows at a considerably slower rate than before.

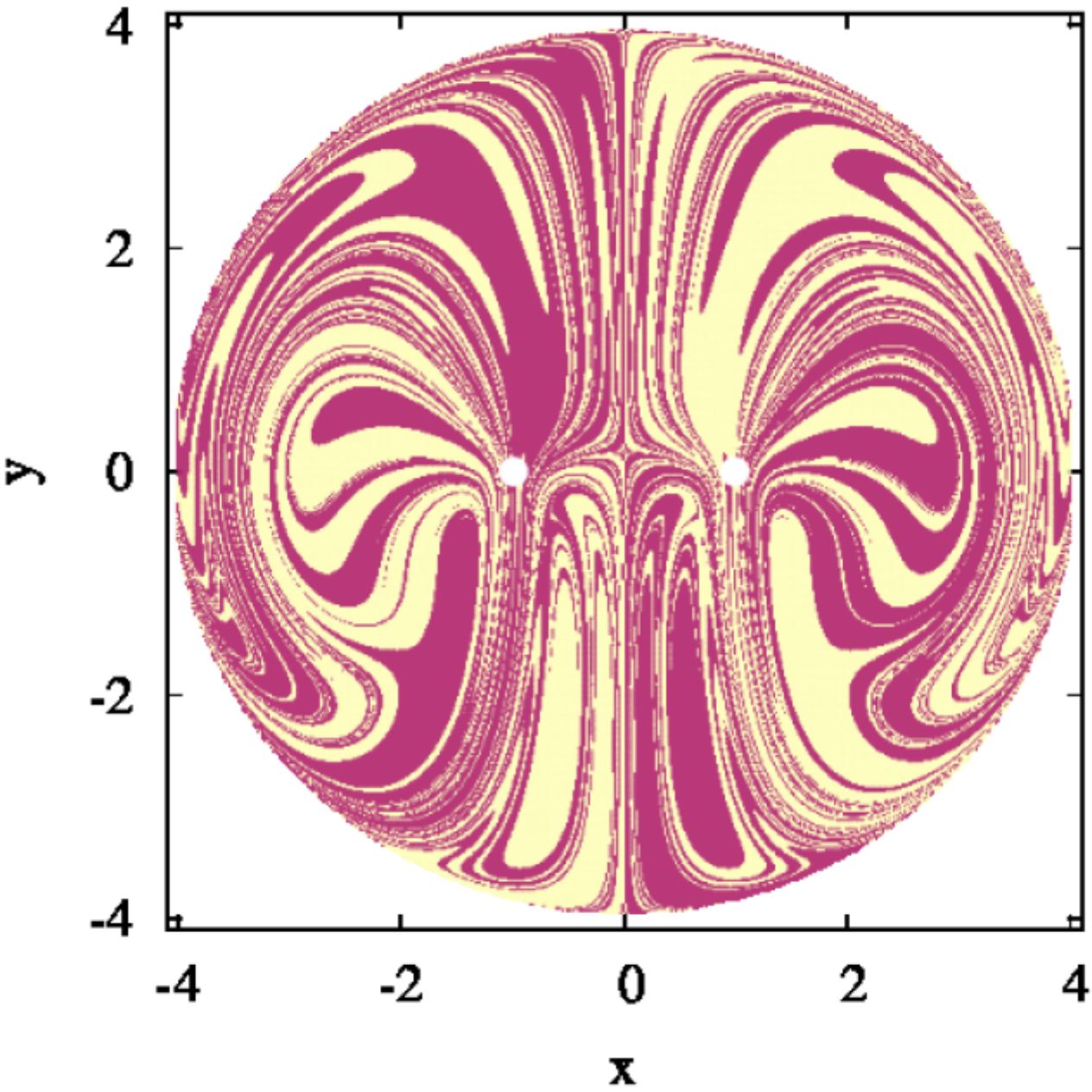


**Figure 15**

Basins of attraction for the two stable fixed points in the x,y plane at a fixed initial energy E = 4, β = 0:05. White dots indicate the locations of the fixed point attractors as x*. The round shape of the accessible region of the phase space follows from the fact that the equipotential lines are nearly circular for high enough energy.

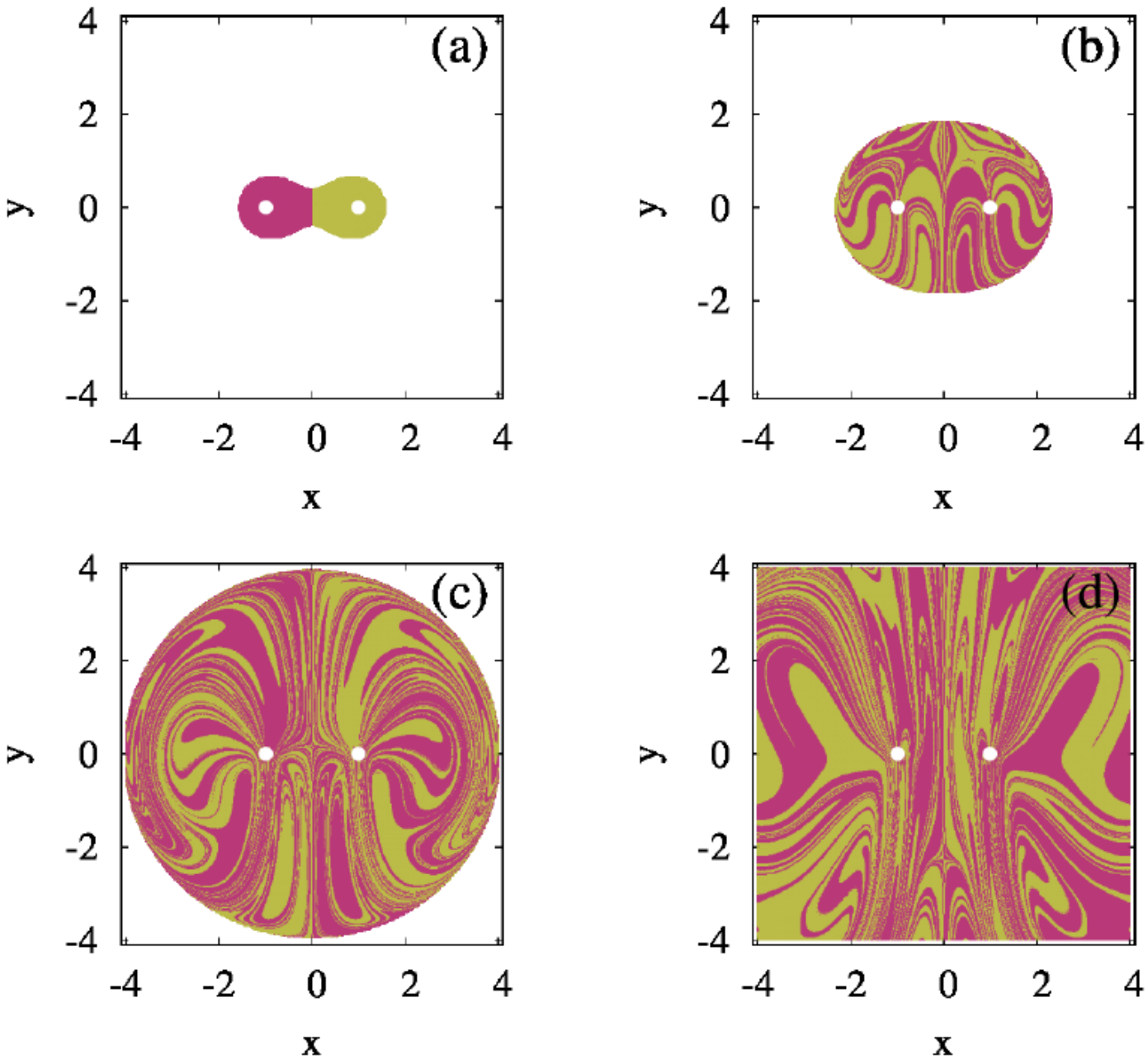


**Figure 16**

Basins of attraction for the two stable fixed points in the x,y plane for various values of the initial energy, (a) E = 2:0, (b) E = 3:0, (c) E = 4:0, (d) E = 5:0. Dissipation is β = 0:05. White dots indicate the locations of the fixed points attractors.

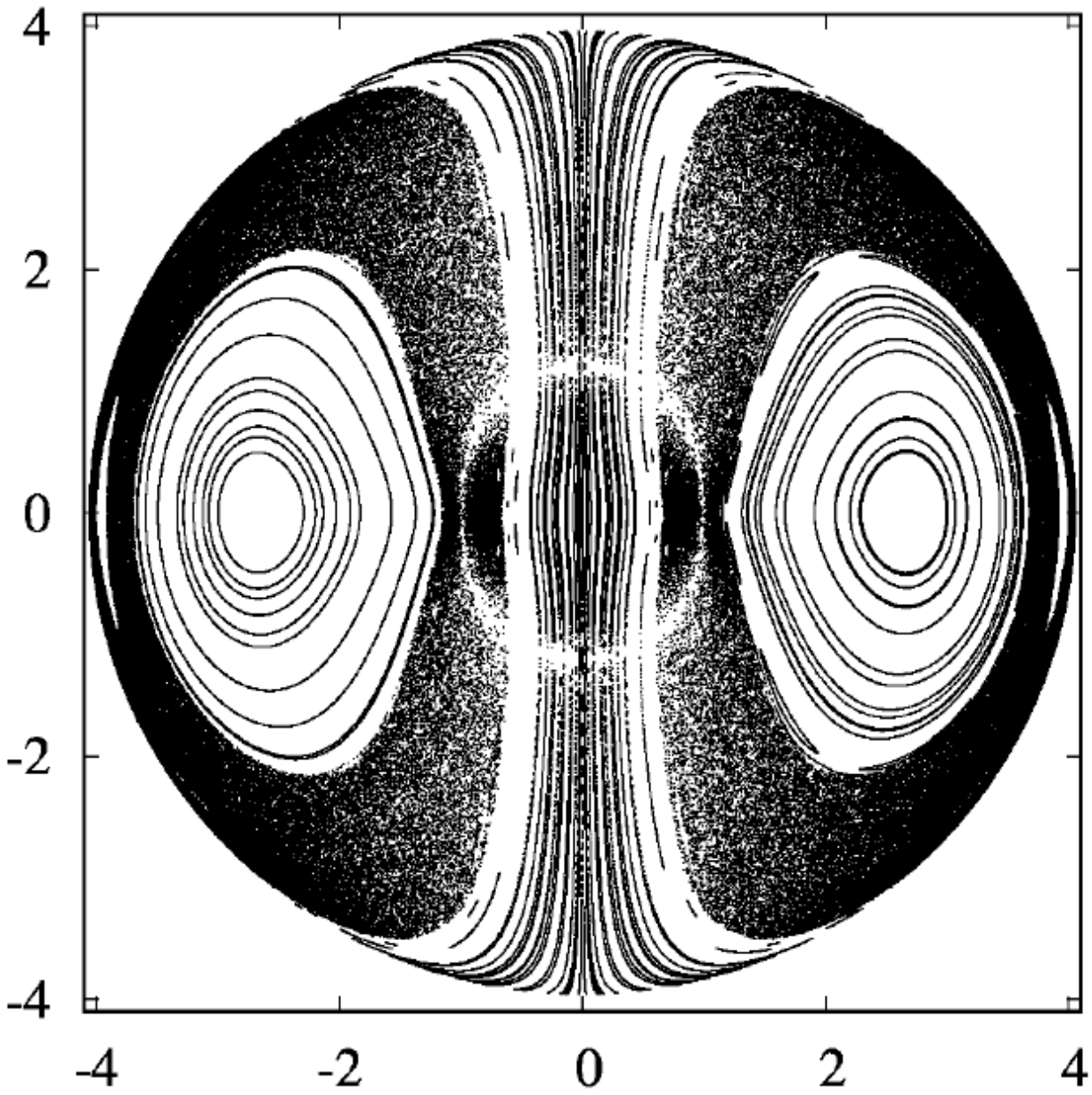


**Figure 17**

The $\dot{x} = 0, \dot{y} > 0$ Poincare section of the magnetic pendulum in the (x,y) plane for trajectories of energy E = 4:0.

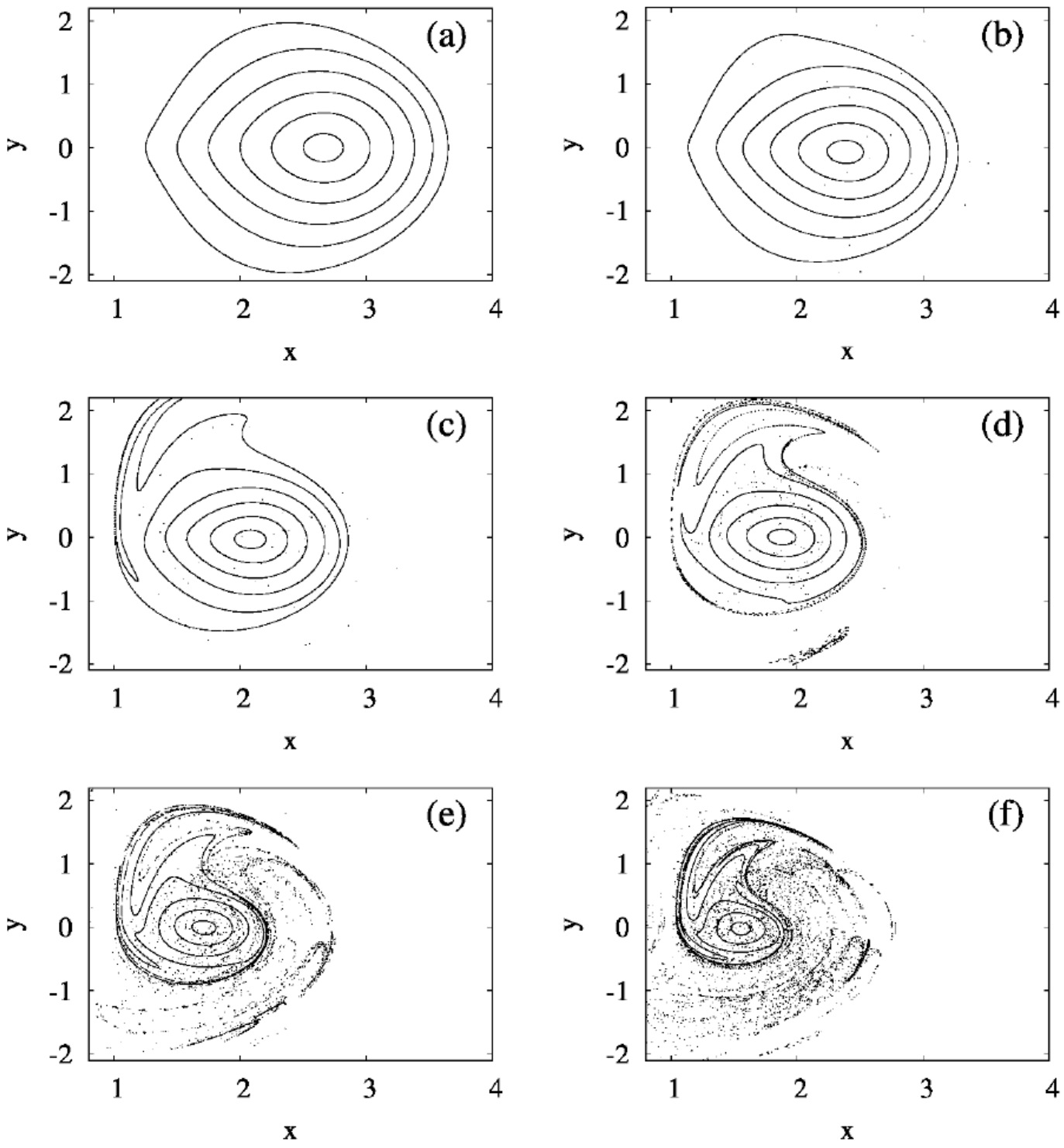


## Figure 18

Subsequent Poincaré sections of 6 KAM tori of the zero dissipation case (a) with damping turned on as β = 0:005 shown after (b) 1, (c) 2, (d) 3, (e) 4, (f) 5 Poincare maps. Note that in the last panels curves intersect each other indicating that the initially planar torus ensembles became essentially threedimensional with the increasing number of steps.

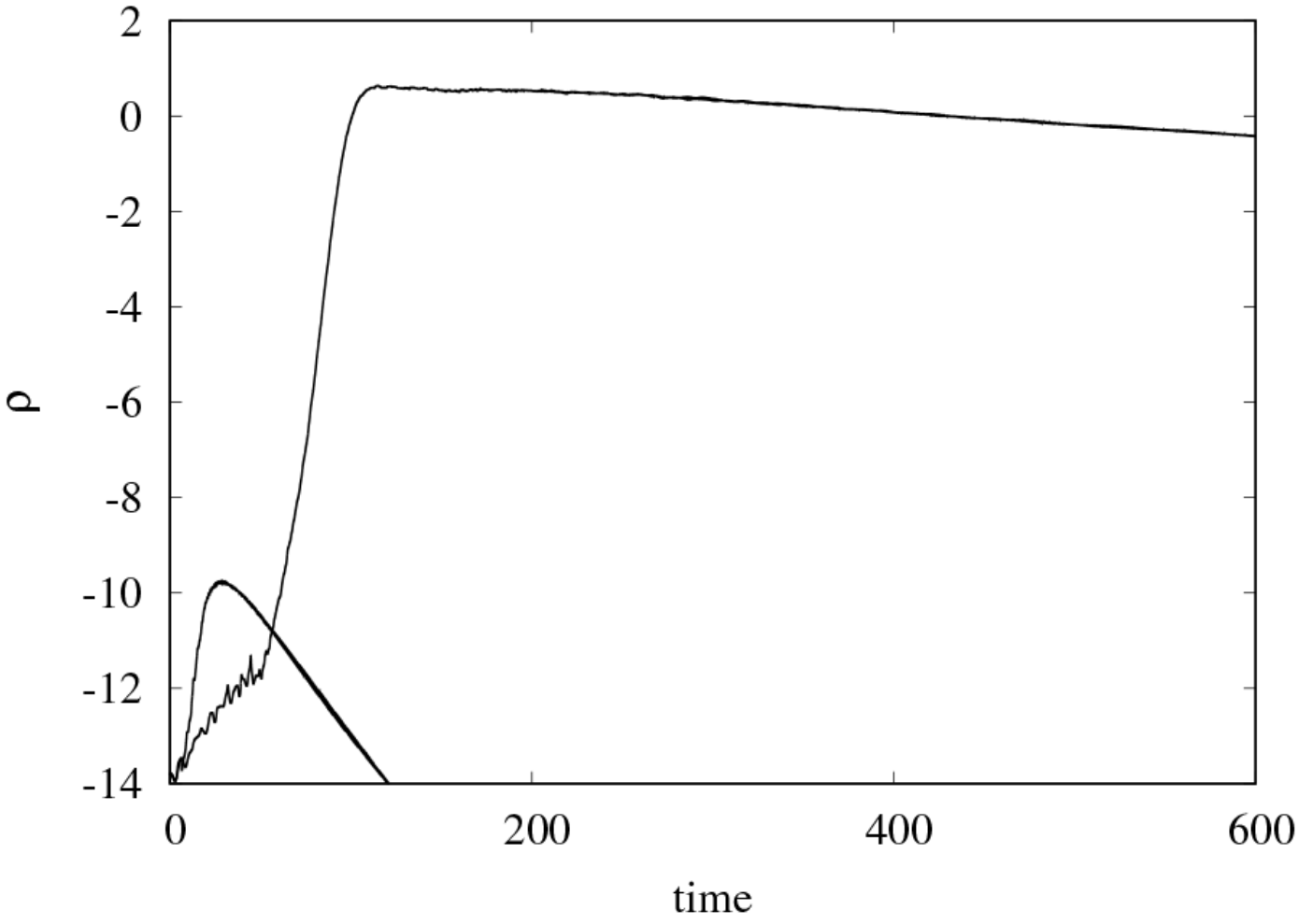


**Figure 19**

EAPD for a single torus, measured at two different values of dissipation β = 0:005 (upper curve) and β = 0:05 (lower curve).

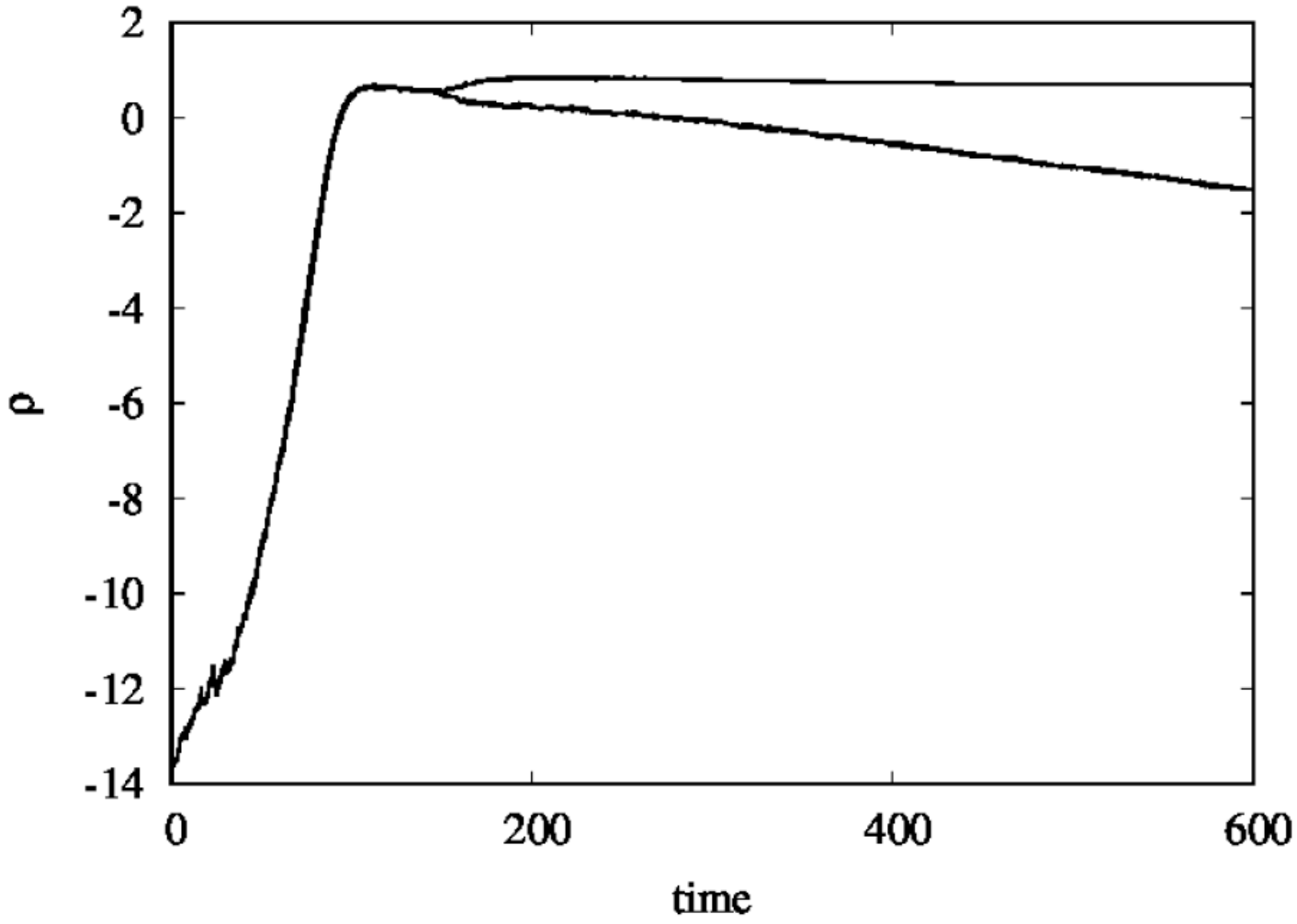


## Figure 20

EAPD for a single torus (outermost in Fig. 18a) for β = 0:005. The two curves correspond to the pairs of points settling to the same (lower curve) or different (upper curve) fixed points.

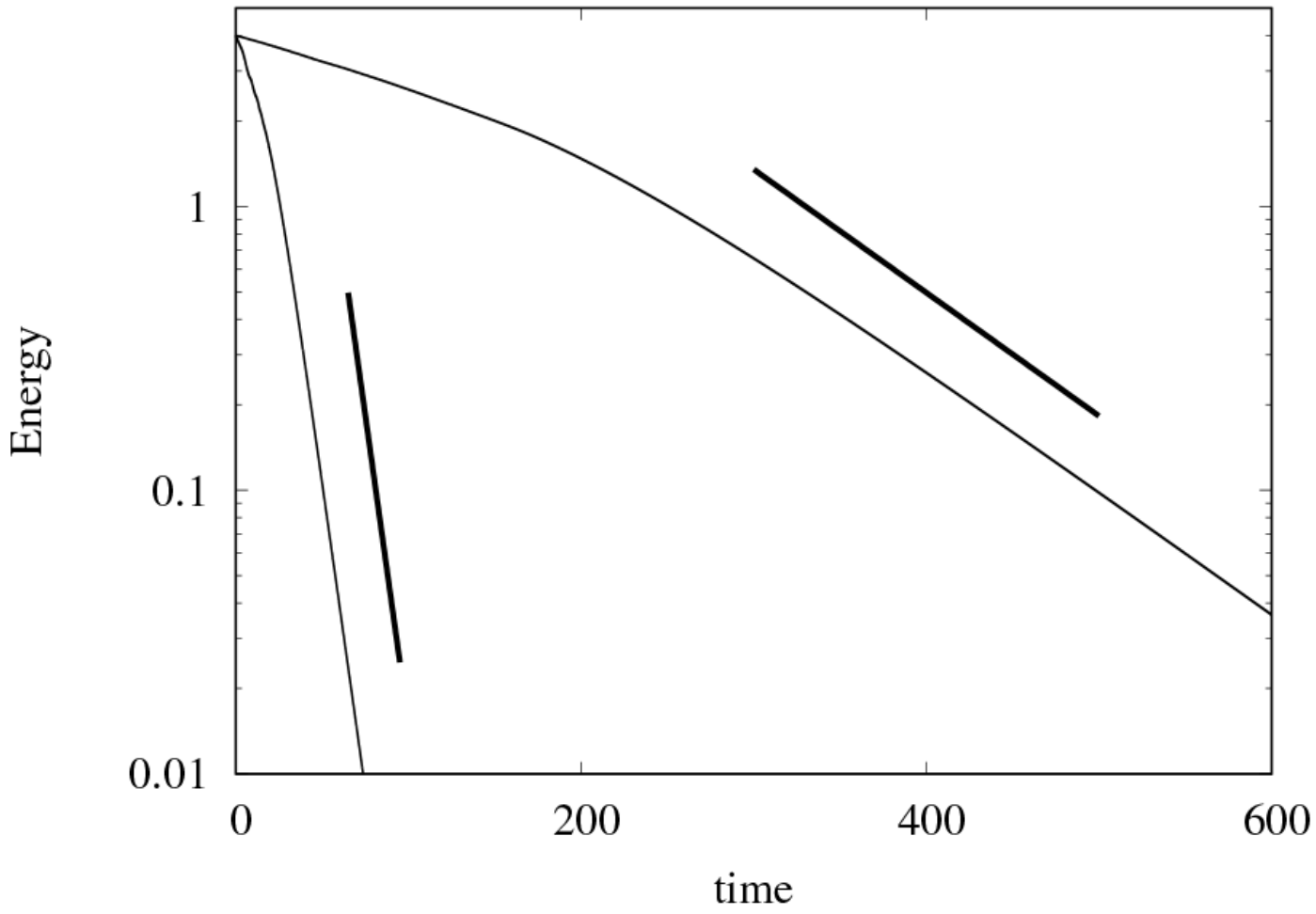


**Figure 21**

The ensemble average of the energy of the pendulum for the points of a single torus, measured at two different values of dissipation β = 0:005 (upper curve) and β = 0:05 (lower curve). Thick lines show the slope −2β for both cases.

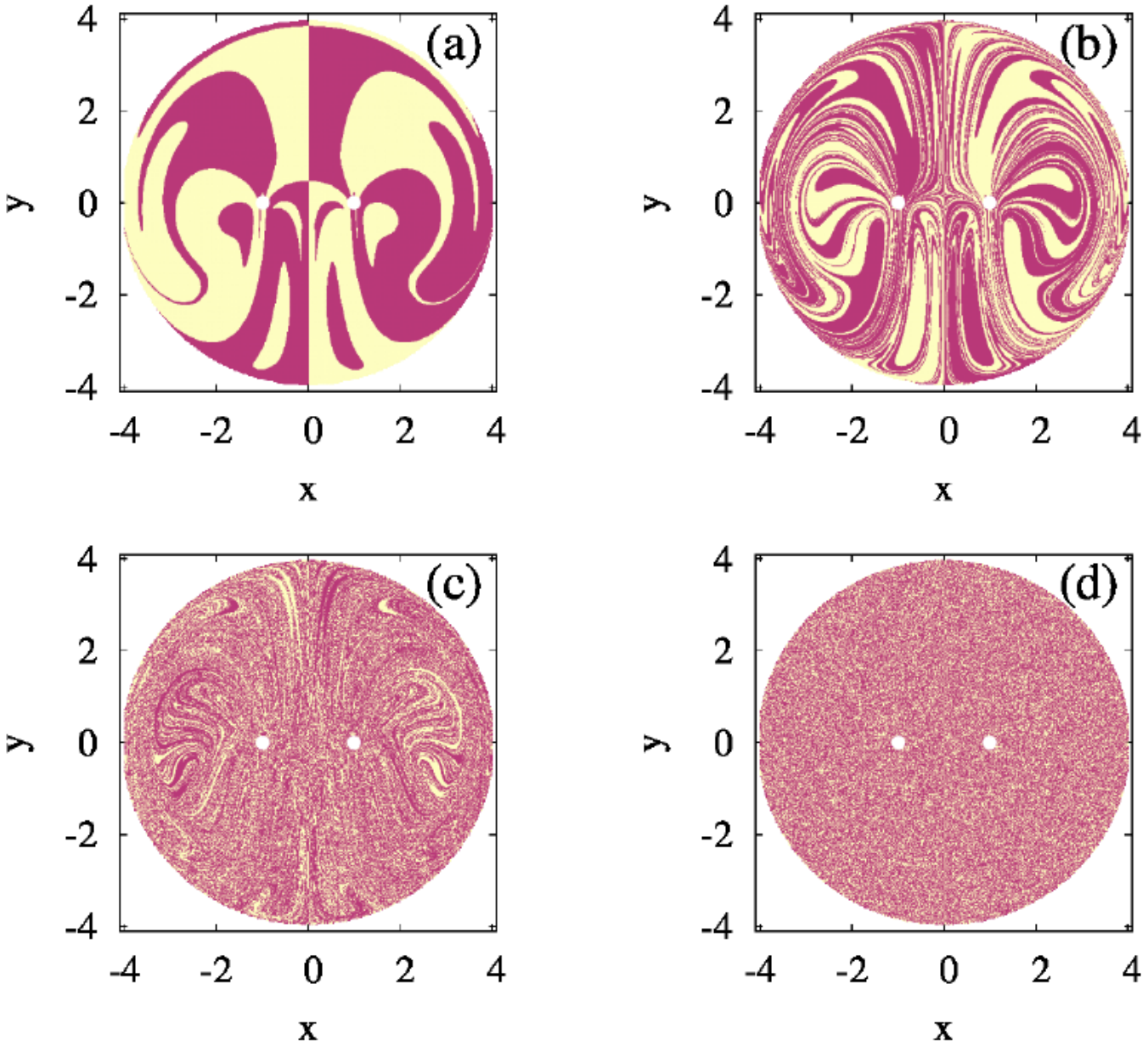


## Figure 22

Basins of attraction for the two stable fixed points in the x,y plane for various values of the dissipation, (a) β = 0:1, (b) β = 0:05, (c) β = 0:025, (d) β = 0:005. The initial energy is E = 4:0. White dots indicate the locations of the fixed point attractors.